Journal of Functional Materials and Applied Engineering

Research Paper

Study on Preparation and Fresh-Keeping Performance of Plant Polyphenol-Nanocellulose Antibacterial Composite Films

Kenneth Thompson [1], **Patricia Brown** [2,*]

[1] Department of Chemistry, Nelson Mandela University, Port Elizabeth, South Africa

[2] Department of Engineering Development and Technology, Aarhus University, Birk Centerpark 15, Building 8001, 7400 Herning, Denmark

*Corresponding author: Kenneth.Thompson@yahoo.com; ppwBrown@btech.au.dk

Abstract. In this work, a TEMPO/NaClO/$NaClO_2$ oxidation system based on 2,2,6,6-tetramethylpiperidin-1-oxyl was adopted to modify bacterial cellulose (BC) for the fabrication of TEMPO-oxidized cellulose nanofibrils (TOCNF). The as-prepared TOCNF was composited with rose polyphenol extract (RPE) to construct multifunctional rBC composite films with outstanding ultraviolet (UV) shielding and antibacterial fresh-keeping capacities. The influence of reaction temperature on TEMPO-mediated oxidation was systematically explored, and comprehensive characterization and analysis were carried out to evaluate the physicochemical properties of the rBC composite films. Experimental results demonstrate that moderately elevating reaction temperature can significantly boost oxidation efficiency. The TOCNF sample prepared at 60 °C (denoted BC-60) achieves a carboxyl content of 1.2 mmol/g. The incorporation of RPE does not destroy the well-ordered three-dimensional network architecture of TOCNF, while remarkably improving the mechanical strength and thermal stability of composite membranes. When the mass ratio of BC-60 to RPE reaches 1:10, the resultant rBC-T composite film delivers optimal overall performance, which can completely block full-spectrum UV light ranging from 200 nm to 400 nm and exert potent antibacterial activity against Escherichia coli. The diameter of inhibition zone reaches (13.02 ± 0.29) mm under a bacterial suspension mass fraction of 0.5%. After 10 days of cold storage at 4 °C, shrimp samples packaged with rBC-T exhibit a significantly lower pH value compared with those wrapped by pure BC-60 TOCNF films, which verifies the superior fresh-preserving capacity of the composite material. This rBC composite film possesses tremendous application potential in the field of functional food packaging.

Keywords: *nanocellulose; rose polyphenol extract; composite film; antibacterial and fresh-keeping performance; UV shielding property*

Received on 02 July 2024, Accepted on 05 Nov 2024, Published on 15 Dec 2024

1 Introduction

Nanocellulose features nanoscale morphological characteristics coupled with excellent physicochemical merits including high crystallinity, superior mechanical strength and large specific surface area, which greatly broaden the application scope of natural cellulose and display promising prospects in biomedicine, food packaging, electronic devices and other industrial sectors. Bacterial cellulose (BC) represents a high-performance natural nanocellulose with enormous development potential. Existing research reveals that BC possesses high polymerization degree and crystallinity, with robust intra- and inter-molecular hydrogen bonds formed within crystalline regions, contributing to outstanding mechanical properties yet poor solubility in conventional solvent systems. Besides, BC surface only carries single hydroxyl functional groups, resulting in limited functional diversity and severely restricting its multi-scenario utilization.

To address the above drawbacks of BC, the TEMPO-catalyzed oxidation system offers an efficient and mild modification pathway. Under mild reaction conditions, TEMPO oxidation can selectively convert the C6 hydroxyl groups (-OH) on cellulose chains into carboxyl groups (-COOH). The oxidation reaction exclusively occurs on fiber surfaces without disrupting the intrinsic micro-morphology and crystal structure of BC, maximally retaining its structural integrity. After TEMPO oxidation, the intermolecular hydrogen bonding of TOCNF is moderately

weakened, enabling uniform and stable dispersion in aqueous media. This modification technology delivers high product yield, and the obtained TOCNF possesses a large aspect ratio. If wood fibers serve as raw materials, non-cellulosic components can be efficiently removed, facilitating intra-fiber delamination and enhancing reagent penetration efficiency.

To further exploit the application potential of TOCNF in food packaging, current research primarily integrates TOCNF with natural bioactive substances to endow the composite materials with antibacterial and antioxidant functions while preserving favorable mechanical performance. Rose polyphenol extract (RPE) is extracted from edible and medicinal rose plants, abundant in structurally diverse polyphenolic bioactive compounds. Previous studies have confirmed that natural plant polyphenols universally exhibit prominent antioxidant and antibacterial capacities. For instance, Bekar et al. optimized the polyphenol extraction process using deep eutectic solvents and verified the antioxidant, neuroprotective and bacteriostatic activities of quince polyphenols. Relevant investigations have also probed the interaction between β-casein in milk and polyphenols, as well as the impact of sterilization treatment on the bioavailability of RPE. Experimental outcomes indicate that RPE can exert potent free radical scavenging and nitrite removal effects via synergistic multi-path oxidation mechanisms.

In view of the above research foundations, this paper adopts the TEMPO/NaClO/$NaClO_2$ oxidation system to introduce carboxyl groups onto BC molecular chains and synthesize TOCNF, followed by optimization of oxidation temperature parameters. On this basis, TOCNF fabricated at different temperatures was blended with RPE, and vacuum filtration was utilized to fabricate multifunctional composite films. This research aims to provide innovative ideas and technical references for the development and industrialization of high-performance active food packaging materials.

2 Materials and Experimental Methods

2.1 Raw Materials and Chemical Reagents

Bacterial cellulose (BC) suspension (mass fraction 1.20%) was purchased from Beijing Yicifang Green Technology Co., Ltd. Fresh rose petals were commercially sourced. Disodium hydrogen phosphate dodecahydrate ($Na_2HPO_4·12H_2O$, analytical grade) was supplied by Xilong Scientific Co., Ltd. 2,2,6,6-tetramethylpiperidin-1-oxyl (TEMPO, 98% analytical grade), sodium dihydrogen phosphate monohydrate ($NaH_2PO_4·H_2O$, 98% analytical grade), sodium chlorite ($NaClO_2$, reagent grade), sodium hypochlorite (effective chlorine ≥60%, analytical grade), and dialysis bags (molecular weight cutoff 200 Da) were all purchased from Shanghai Macklin Biochemical Co., Ltd. Unless otherwise specified, all other chemical reagents were domestic analytical grade. Ammonia-free distilled water and deionized water were self-prepared in the laboratory.

Preparation of RPE: Dried rose petals were extracted with 40 wt% ethanol aqueous solution, followed by concentration and freeze-drying to obtain solid rose polyphenol extract powder.

2.2 Experimental Procedures

2.2.1 Fabrication of TOCNF

Preparation of phosphate buffered saline (PBS): 3.32 g $Na_2HPO_4·12H_2O$ was dissolved in deionized water to prepare Solution A; 1.48 g $NaH_2PO_4·H_2O$ was dissolved in deionized water to prepare Solution B. 9.26 mL Solution A and 10.74 mL Solution B were fully mixed to formulate 20 mL PBS buffer with pH=7.14.

20 mL PBS buffer was added into 100 mL BC suspension, then diluted with deionized water to a total volume of 200 mL. Sequentially add 0.032 g TEMPO and 2.26 g $NaClO_2$, and carry out light-shielded stirring reactions for 96 h at 20 °C and 60 °C respectively. After reaction completion, the mixed solution was dialyzed for 48 h to eliminate unreacted chemical reagents. The dialyzed product was concentrated and freeze-dried to measure solid content. The TOCNF samples prepared at 20 °C and 60 °C were labeled BC-20 and BC-60 correspondingly.

2.2.2 Fabrication of TOCNF-RPE Composite Films

3 g of 1.0 wt% BC, BC-20 and BC-60 suspensions were separately dispersed in 100 mL deionized water and

homogenized. Vacuum filtration was performed to prepare pure BC film and two pure TOCNF films, designated BC-0, BC-t and BC-T.

3 g of 1.0 wt% BC-20 and BC-60 suspensions were mixed with RPE at mass ratios of 1:1, 1:5 and 1:10 respectively, dispersed in 100 mL deionized water and fully blended. The mixed system was stirred away from light for 24 h, then vacuum-filtered to obtain rBC composite films. Composite films derived from BC-20 were named rBC-t_1, rBC-t_5, rBC-t_{10}; those fabricated from BC-60 were marked rBC-T_1, rBC-T_5, rBC-T_{10}.

2.3 Characterization and Testing Methods

2.3.1 Quantification of Carboxyl (-COOH) Content in TOCNF

Conductometric titration was adopted to measure the carboxyl content (C, mmol/g) of TOCNF, calculated via Formula (1): 30 mL deionized water and 5 mL 0.01 mol/L NaCl solution were added into 10 mL TOCNF suspension. The pH value of the mixture was adjusted to 2.5 using 0.1 mol/L hydrochloric acid, then titrated with 5 mmol/L NaOH solution until pH reached 11. Record the consumed volume of NaOH, pH variation and conductivity data throughout the titration process.

$$C = \frac{(V_1 - V_2)M_{NaOH}}{m}$$

Where: V_1 = Volume of NaOH solution consumed at carboxyl neutralization endpoint (L); V_2 = Volume of NaOH solution consumed for excess HCl neutralization (L); M_NaOH = Molar concentration of NaOH titrant (mol/L); m = Absolute dry mass of TOCNF contained in 10 mL suspension (g).

2.3.2 Physicochemical Characterization of rBC Composite Films

Film thickness was measured at six random positions on each composite membrane using a digital micrometer with 0.001 mm precision, and average thickness was calculated. A SC-80C colorimeter (Beijing Kangguang Optical Instrument Co., Ltd.) was utilized to test color parameters, and total color difference ΔE was calculated via Formula (2). Larger ΔE values indicate more significant color deviation from the reference sample.

$$\Delta E = \sqrt{(L_s - L^*)^2 + (a_s - a^*)^2 + (b_s - b^*)^2}$$

Where: L*, a*, b* = Color parameters of tested rBC films; L_s, a_s, b_s = Color parameters of standard reference sample.

After vacuum gold sputtering treatment, SU8010 scanning electron microscope (Hitachi, Japan) was used to observe micro-morphology of composite films. Nicolet iS5 Fourier transform infrared spectrometer (Thermo Fisher Scientific, USA, ATR mode, wavenumber range 400–4000 cm^{-1}) and AXIS Supra X-ray photoelectron spectrometer (Kratos Analytical, UK) were employed to analyze chemical structures. D8 Advance X-ray diffractometer (Bruker, Germany) was applied for crystalline structure analysis with scanning range 5°–50°, scanning rate 2 °/min, voltage 45 kV, current 40 mA. DTG-60A thermogravimetric analyzer (Shimadzu, Japan) was adopted for thermal stability testing under N_2 atmosphere, temperature range 50–800 °C, heating rate 20 °C/min. WDS-10KN universal tensile tester (MTS, USA) measured mechanical properties, sample dimension 20 mm × 10 mm, tensile rate 20 mm/min, six parallel tests for average value calculation.

2.3.3 UV Blocking and Antibacterial Performance Tests

Lambda 35 UV-Vis spectrophotometer (PerkinElmer, USA) measured UV transmittance to quantify the UV shielding capacity of composite films.

The antibacterial assay followed the protocol reported by Otoni et al.. Escherichia coli (ATCC8099, Gram-negative) and Staphylococcus aureus (ATCC6538, Gram-positive) were selected as test strains, with bacterial suspension mass fractions set at 0.5%, 1% and 2%. Bacteria were inoculated on nutrient agar medium and incubated for 24 h. Circular film samples with 6 mm diameter were placed on agar surfaces and incubated overnight at 37 °C. Experimental groups included blank control (BC-0), pure TOCNF control (BC-T), and experimental rBC-t_1, rBC-t_{10},

rBC-T_1, rBC-T_{10}. Vernier caliper with 0.01 mm precision measured inhibition zone diameters, three parallel replicates for each group. SPSS 26.0 software conducted one-way ANOVA, with $P<0.05$ defined as statistically significant difference.

2.3.4 Fresh-Keeping Application Test of rBC Composite Films

BC-T packaging served as control group and rBC-T_{10} as experimental group for fresh shrimp preservation experiments under 25 °C (ambient) and 4 °C (refrigerated) conditions. Storage durations were set as 0, 1, 3, 7, 10 days, and shrimp pH value was adopted as evaluation indicator. Three parallel samples for each group, 5 g shrimp muscle tissue weighed per sample, homogenized with 20 mL ammonia-free distilled water, stood for 10 min before supernatant pH measurement, each sample tested twice for averaged results.

3 Results and Discussion

3.1 Carboxyl Content of TOCNF

Table 1 lists the carboxyl content data of BC-20 and BC-60. The carboxyl concentrations of TOCNF prepared at 20 °C and 60 °C were (0.49±0.07) mmol/g and (1.00±0.17) mmol/g respectively, consistent with published literature. During TEMPO-mediated oxidation of BC suspension, carboxyl groups are selectively grafted onto cellulose chains to achieve targeted functionalization, producing translucent TOCNF dispersions with excellent dispersion stability and enhanced chemical reactivity. Obvious discrepancies exist in carboxyl content at different reaction temperatures; elevated temperature accelerates oxidation reactions and raises carboxyl loading, which demonstrates that precise temperature control is critical for TEMPO oxidation procedures.

Table 1 Carboxyl Content of TOCNF Synthesized at Different Temperatures (Unit: mmol/g)

Sample Label	Carboxyl Content
BC-20	0.49±0.07
BC-60	1.00±0.07

3.2 Physicochemical Properties of Pure TOCNF Films

3.2.1 Microstructural Morphology

Figure 1 displays SEM images of BC-t and BC-T pure TOCNF membranes. Both films present regular three-dimensional fiber networks after TEMPO oxidation treatment. Compared with BC-t, BC-T exhibits significantly larger pore sizes and looser fiber stacking. This phenomenon illustrates that high-temperature TEMPO oxidation facilitates full separation of individual cellulose nanofibrils and improves the overall structural integrity of materials.

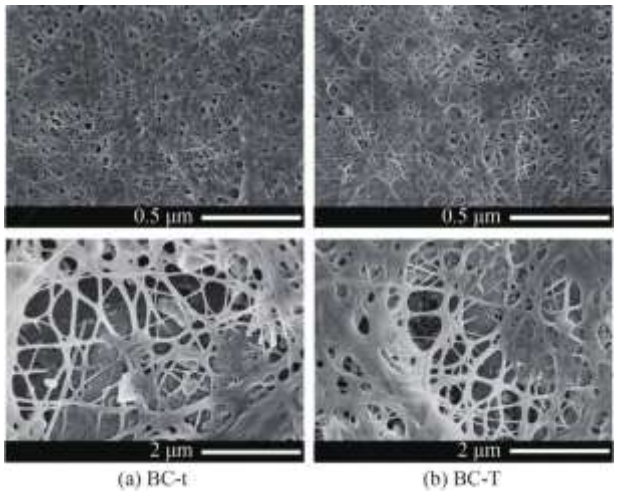

DOI:

Figure 1 SEM images of pure TOCNF films

3.2.2 Chemical Structure Analysis

FT-IR spectra of BC-0, BC-t and BC-T are shown in Figure 2(a). Distinct characteristic absorption peak variations can be observed among three samples. The broad absorption band ranging from 3200 to 3500 cm^{-1} corresponds to stretching vibration of cellulose hydroxyl groups, while the new peak at 1703 cm^{-1} is attributed to carbonyl C=O stretching vibration, verifying selective oxidation of C6 hydroxyl groups into carboxyl groups without eliminating intrinsic hydroxyl groups on cellulose chains, which matches the research conclusions of Isogai et al..

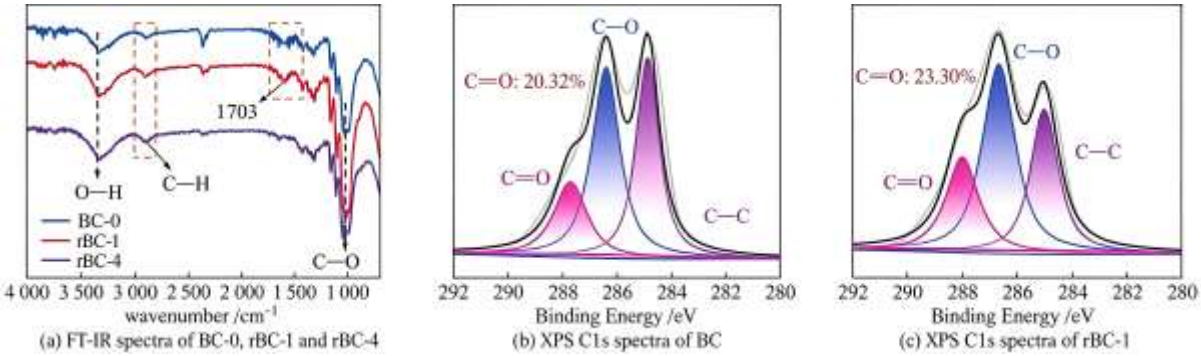

Figure 2 FT-IR spectra of BC-0 and pure TOCNF films and XPS C 1s resolution spectra of pure TOCNF films

XPS semi-quantitative surface functional group analysis was performed on two pure TOCNF films, with C 1s high-resolution spectra presented in Figure 2(b) and (c). The C 1s spectrum of BC-t can be deconvoluted into three peaks corresponding to C–C/C–H, C–O and C=O bonds, further confirming successful grafting of carboxyl groups onto cellulose backbones. When oxidation temperature rises from 20 °C to 60 °C, the peak area ratio of C=O (characteristic of carboxyl groups) increases from 20.32% to 23.30%, proving that reaction temperature acts as a core regulating parameter to accelerate TEMPO oxidation efficiency.

3.2.3 Thermal and Mechanical Properties

TG and DTG curves of BC-0, BC-t and BC-T are displayed in Figure 3(a)(b), and stress-strain curves are shown in Figure 3(c). Mass loss below 200 °C mainly originates from water evaporation within film matrices. The total mass loss ratios of BC-0, BC-t and BC-T are 72.0%, 58.2% and 61.3% separately. After TEMPO oxidation, the initial decomposition temperatures of BC-t (270 °C) and BC-T (280 °C) increase by 20 °C and 30 °C compared with BC-0 (250 °C). Their maximum thermal decomposition temperatures also shift from 330 °C (BC-0) to 350 °C and 365 °C respectively, which indicates that TEMPO oxidation moderately enhances the thermal stability of cellulose films.

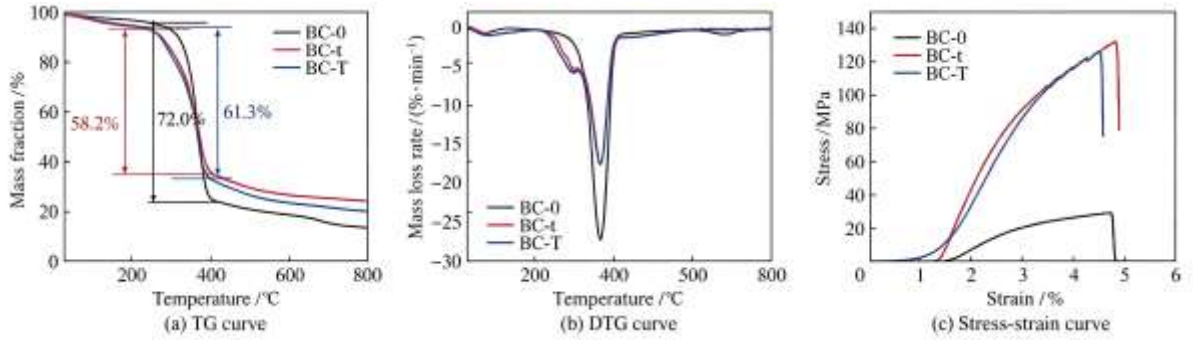

Figure 3 TG, DTG, and stress-strain curves of BC-0 and pure TOCNF films

In terms of mechanical performance, the tensile strength of pure TOCNF films greatly surpasses BC-0 (32.6 MPa). Compared with the blank BC-0 sample, the tensile strength of BC-t (20 °C oxidation) and BC-T (60 °C oxidation) increase by 110.1% and 132.5% correspondingly. This improvement arises from more ordered, uniform three-dimensional fiber network arrangement after oxidation, forming evenly distributed intermolecular hydrogen

bonds and higher stress transfer efficiency under external force loading.

3.3 Physicochemical Properties of rBC Composite Films

3.3.1 Micro-Morphology of Composite Membranes

Figure 4(a)–(c) show SEM images of rBC-t composite films with different BC-20/RPE mass ratios. Adjusting RPE addition amount does not alter the intrinsic fiber morphology of BC-20, which means the addition of polyphenol extract can retain the intact skeleton structure of nanocellulose. In contrast with pure BC-t film, rBC composite membranes incorporated with RPE exhibit narrowed network pores and tighter fiber interweaving.

Figure 4(d)–(f) illustrate SEM graphs of rBC-T composite films with varied BC-60/RPE ratios. Minor agglomeration of polyphenol particles appears in rBC-T_5 and rBC-T_{10} samples. As RPE dosage increases, fiber arrangement disorder degree rises, finally forming dense network structures with tiny pores. Comprehensive morphological comparison of two series of composite films reveals that phenolic hydroxyl groups on RPE molecules can crosslink with carboxyl groups on TOCNF surfaces to reinforce the overall fiber network structure.

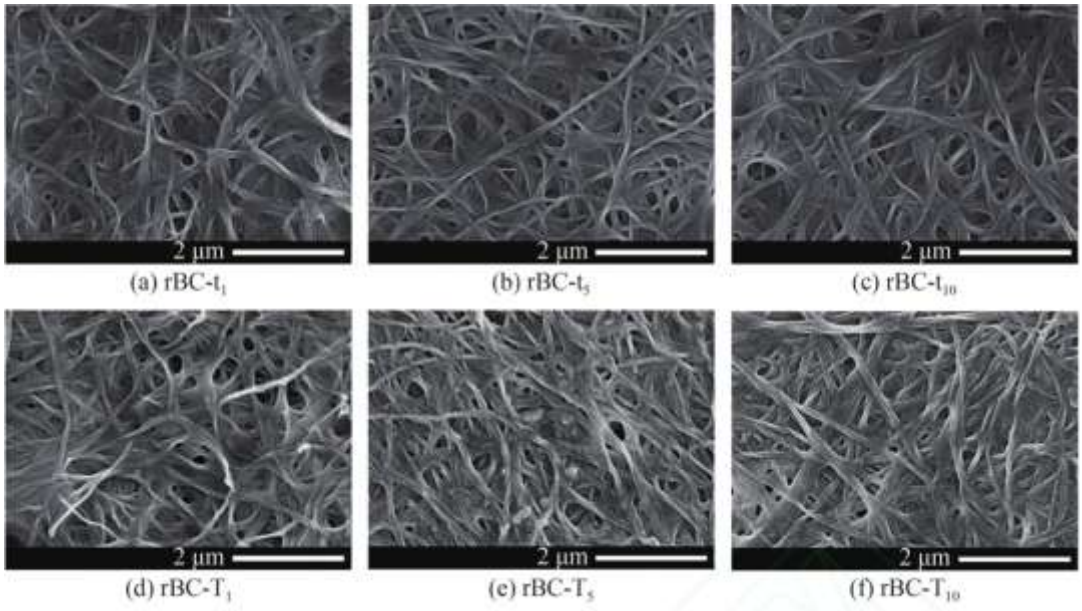

Figure 4 SEM images of rBC composite films with different RPE addition amount

3.3.2 Crystalline and Chemical Structure of rBC Films

Since TEMPO oxidation only occurs on cellulose surface layers, TOCNF can maintain the high crystallinity and crystal width of original BC fibers. XRD patterns of BC-t and rBC composite films are displayed in Figure 5(a). No new diffraction peaks or peak position shifts are observed after RPE incorporation, demonstrating that polyphenol additives will not destroy the ordered crystalline framework of TOCNF. Relevant research states that crosslinking between phenolic hydroxyl groups of RPE and carboxyl groups of TOCNF reduces the accessibility of polyphenol molecules to cellulose crystal regions, thus avoiding damage to cellulose I crystal lattice.

FT-IR spectra of rBC-t and rBC-T are shown in Figure 5(b)(c). No obvious shift occurs to characteristic cellulose absorption peaks after RPE doping. Absorption bands at 1200–1300 cm^{-1} correspond to C–O and C–C stretching vibrations; the peak at 1550 cm^{-1} is assigned to benzene ring skeleton vibration, and the band near 1026 cm^{-1} originates from aromatic C–H bending vibration. The appearance of typical polyphenol characteristic peaks confirms stable loading of RPE within TOCNF matrix via non-covalent crosslinking interactions.

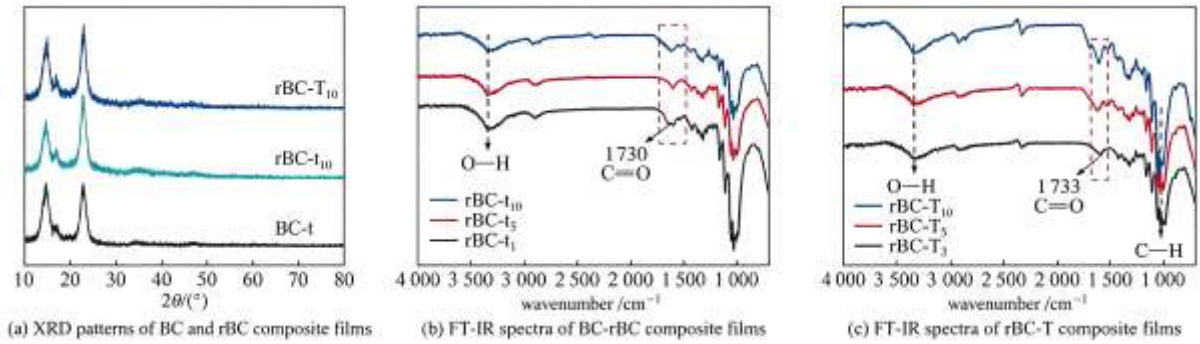

Figure 5 XRD patterns of BC-t and rBC composite films, and FT-IR spectra of rBC composite films

3.3.3 Thermal Stability of rBC Composite Films

TG and DTG curves of rBC series membranes are presented in Figure 6. All composite films with RPE exhibit thermal degradation trends similar to pure TOCNF samples in Figure 3. The total mass loss ratio decreases with the increase of RPE content. Under identical polyphenol addition levels, rBC-T films display lower mass loss than rBC-t counterparts. This phenomenon is attributed to higher carboxyl content of BC-60 prepared at high temperature, which forms abundant hydrogen bonds with phenolic hydroxyl groups of RPE, facilitating homogeneous dispersion of polyphenols inside fiber networks and delivering superior thermal resistance.

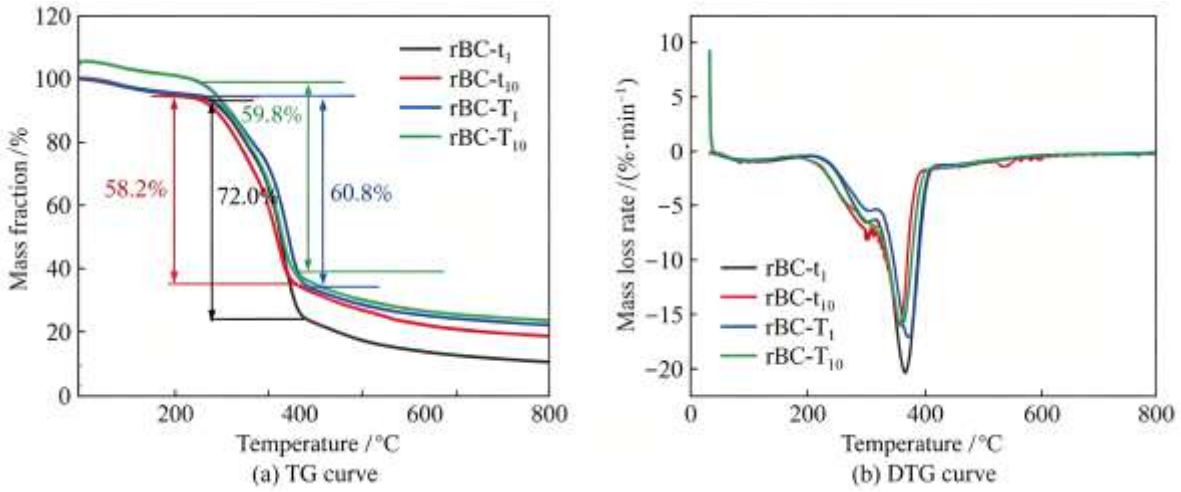

Figure 6 TG and DTG curves of rBC composite films

3.3.4 Mechanical Performance of rBC Composite Films

Tensile strength data of rBC membranes are summarized in Figure 7.

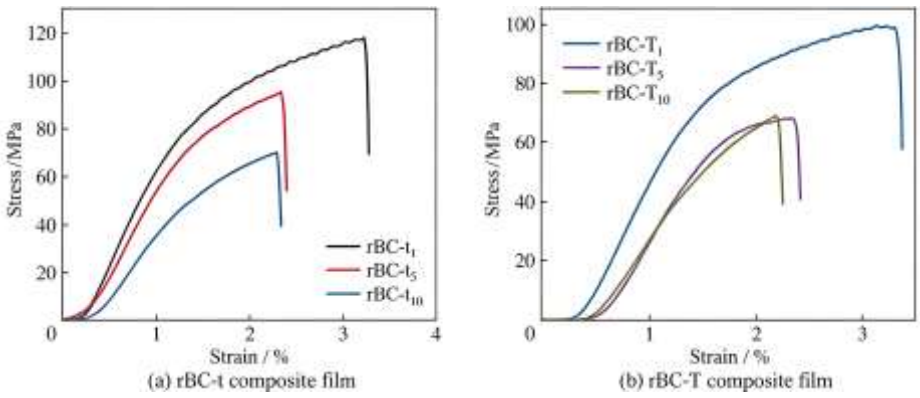

Figure 7 Stress-strain curves of rBC composite films

The addition of RPE does not weaken the mechanical properties of composite films. Phenolic hydroxyl groups on polyphenol molecules form extensive hydrogen bonding crosslinks with hydroxyl and carboxyl groups of TOCNF, enabling uniform dispersion of RPE to fill micro-pores between nanofibers and construct denser film structures, thus improving hardness and structural stability. This result is consistent with prior research conclusions: polyphenol-rich extract fillers can form strong interfacial interactions with cellulose polymer chains to restrict molecular chain slippage and enhance film rigidity after homogeneous dispersion.

3.3.5 Optical and UV-Shielding Properties

Digital photos and color parameter data of BC-0, pure TOCNF and rBC composite films are shown in Figure 8 and Table 2. Pure BC and TOCNF films possess high L* (lightness) values with low a* (red-green axis) and b* (yellow-blue axis) values. After RPE incorporation, L* continuously decreases while a* and b* rise with increasing polyphenol dosage, which means composite films gradually darken with intensified red and yellow tones and finally turn tawny. Precise color regulation can be realized by adjusting RTE addition amount to satisfy diverse appearance requirements of packaging materials.

Table 2 Thickness and chromatic values of BC-0, pure TOCNF films, and rBC composite films

Film Sample	Thickness /mm	L*	a*	b*	ΔE
BC-0	0.028	61.31	-0.67	-1.66	61.34
BC-t	0.017	47.28	-0.68	-4.91	47.54
BC-T	0.016	47.25	-0.52	-3.97	47.42
rBC-t_1	0.028	53.43	-0.18	2.29	53.48
rBC-t_5	0.031	43.84	0.18	6.20	44.28
rBC-t_{10}	0.038	36.25	5.24	6.49	37.20
rBC-T_1	0.025	41.55	-0.30	1.51	41.58
rBC-T_5	0.035	37.52	2.77	4.02	37.84
rBC-T_{10}	0.044	39.85	8.72	6.78	24.90

L*: Lightness value; a*: Red-green chromatic coordinate; b*: Yellow-blue chromatic coordinate; ΔE: Total color difference

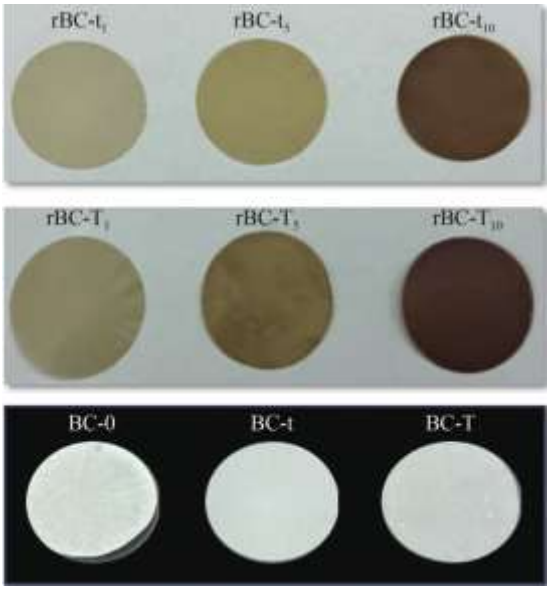

Figure 8 Photos of BC-0, pure TOCNF films, and rBC composite films

Plant-derived flavonoids and polyphenols are ideal UV-blocking raw materials with non-toxicity and excellent biocompatibility, such as chebula tannins which integrate UV shielding and antioxidant capacities. UV-Vis spectroscopy serves as the standard quantitative method to evaluate UV resistance: lower light transmittance indicates stronger UV interception capacity. Aromatic conjugated double bonds and intramolecular hydrogen bonds of polyphenols synergistically capture UV photons, endowing RPE-containing films with wide UV blocking prospects. UV transmittance curves of all samples are plotted in Figure 9. Compared with BC-0 and pure TOCNF films, all rBC composite films display drastically reduced UV transmittance. As RPE loading increases, transmittance at 420 nm approaches zero, which proves the outstanding UV absorption performance of rose polyphenols originating from conjugated aromatic structures within molecules.

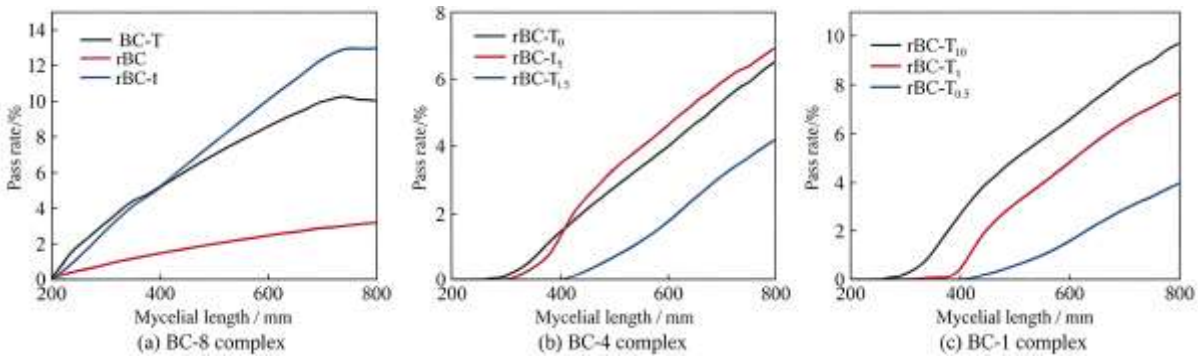

Figure 9 UV transmittance of BC-0, pure TOCNF films, and rBC composite films

3.3.6 Antibacterial Activity of rBC Composite Films

Inhibition zone tests were conducted to evaluate bacteriostatic capacity, and photos of agar plates are displayed in Figure 10. No obvious inhibition zones are observed around BC-0 and BC-T control groups, which verifies that all antibacterial activity of rBC composite films originates from incorporated RPE.

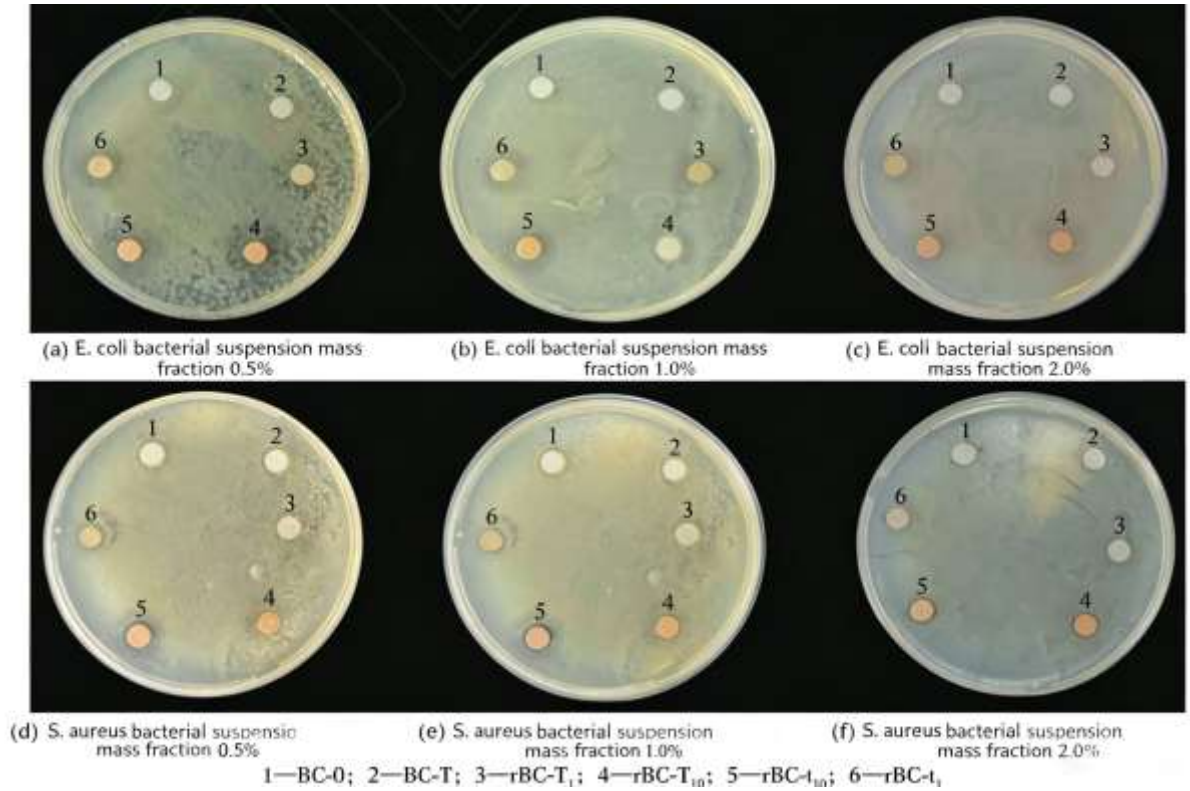

Figure 10 Photos of antibacterial zones for rBC composite films with different RPE addition amount

From Figure 10(a)–(c), the antibacterial effect against E. coli positively correlates with RPE dosage. Under 0.5 wt% bacterial suspension concentration, the inhibition zone diameter of rBC-t_{10} reaches (13.02±0.29) mm, significantly larger than rBC-t_1 (8.18±0.23 mm, $P<0.05$). The inhibition zone of rBC-T_{10} also surpasses rBC-T_1 remarkably. Moreover, rBC-T series films exhibit slightly stronger bacteriostatic effects than rBC-t counterparts under identical polyphenol content, because high-temperature oxidized BC-60 carries higher carboxyl density, forming more stable hydrogen bonds with RPE to realize slow uniform release of polyphenols within fiber networks. When E. coli concentration rises to 1.0 wt%, inhibition zone diameters shrink moderately, yet rBC-t_{10} and rBC-T_{10} still retain effective antibacterial effects. At 2.0 wt% bacterial concentration, all composite films show indistinct inhibition zones (diameter <7.00 mm), indicating that the bacteriostatic performance of RPE is limited by bacterial concentration and only exerts remarkable suppression on low-density E. coli populations.

Previous research on tea polyphenol-cellulose composite films demonstrated that the inhibition zone diameter of composite membranes shows no significant difference compared with equivalent pure polyphenol solution, with uniformly diffused bacteriostatic regions, proving polyphenols must leach out from film substrates to execute antibacterial functions. Similar conclusions are obtained from anthocyanin-starch packaging films: plant bioactive components physically load on cellulose via hydrogen bonds without chemical bonding, and gradually diffuse into surrounding medium with extended incubation time. These experimental rules match our test results: rBC inhibition zones display uniform distribution without edge enrichment, and zone diameter expands with increased RPE dosage. Combined with FT-IR characterization confirming non-covalent interactions between TOCNF and RPE, this provides structural basis for polyphenol diffusion. The antibacterial mechanism of rose polyphenols relies on direct contact with bacterial cell membranes, requiring molecular diffusion to reach bacterial surfaces for inhibitory effects. The diameter of inhibition zones far exceeds the 6 mm film sample size in Figure 10, further validating that antibacterial polyphenols continuously leach out rather than merely staying on film surfaces.

Figure 10(d)–(f) reveal that all film samples barely exert inhibitory effects on S. aureus, resulting from structural differences between Gram-positive and Gram-negative bacterial cell walls. E. coli (Gram-negative) only possesses a thin 2–3 nm peptidoglycan layer and loose outer phospholipid bilayer membrane, allowing flavonoid and phenolic molecules of RPE to easily penetrate intracellular compartments. By contrast, S. aureus (Gram-positive) features a dense 20–80 nm thick peptidoglycan cell wall rich in teichoic acid, forming steric hindrance that blocks polyphenol permeation and eliminates bacteriostatic effects.

Comprehensive analysis proposes three antibacterial pathways of rBC composite films against E. coli:

Phenolic hydroxyl groups of leached polyphenols generate hydrogen bonding and hydrophobic interactions with lipid bilayers of E. coli membranes, disrupting membrane integrity and permeability, leading to leakage of intracellular electrolytes and nutrients to inhibit bacterial proliferation.

Phenolic hydroxyl groups are prone to oxidation into quinone intermediates, inducing excessive reactive oxygen species (ROS) accumulation inside bacteria to trigger intracellular oxidative stress, damaging proteins and nucleic acids and blocking normal metabolic cycles.

Polyphenol molecules bind active sites of key metabolic enzymes (dehydrogenase, protease) on bacterial membranes, suppressing enzyme catalytic activity and interfering energy and substance biosynthesis of bacteria.

3.3.7 Fresh-Keeping Performance of rBC-T_{10} Composite Film

During seafood storage, shrimp proteins degrade under combined effects of microbial reproduction and endogenous enzymes, generating alkaline ammonia and amine metabolites that continuously elevate shrimp pH, which can serve as a direct indicator of spoilage degree. Photos and pH variation curves of shrimp samples packaged with BC-T and rBC-T_{10} under 25 °C and 4 °C are shown in Figure 11. The initial pH of all shrimp samples stabilizes around 7.5 and gradually rises with prolonged storage time, yet distinct growth rates exist between different packaging groups.

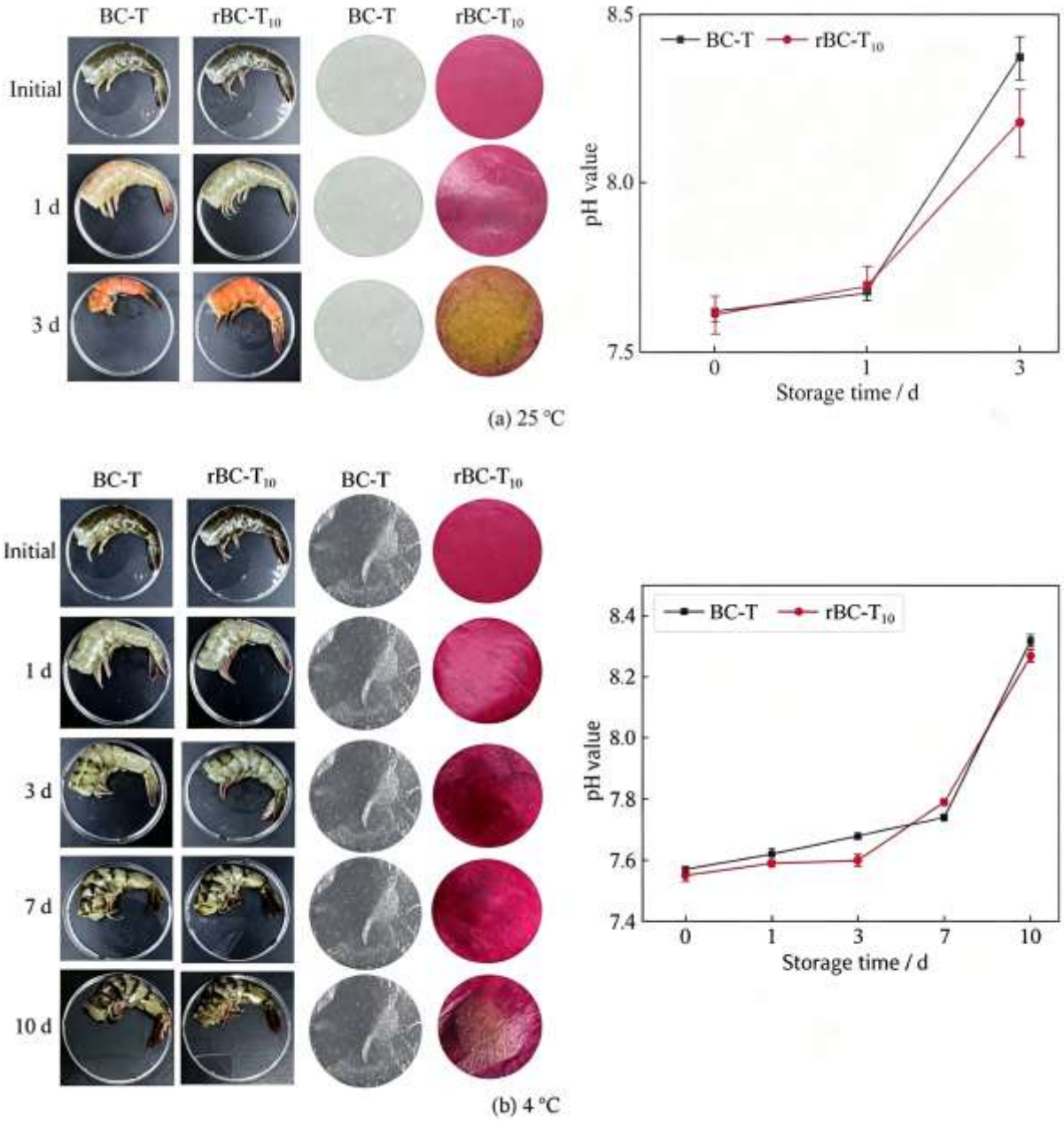

Figure 11 Photos of fresh shrimp preserved using BC-T and rBC-T10, and changes in the pH of the fresh shrimp samples

At 25 °C, the pH of BC-T packaged shrimp rises to 8.4 after 3 days of storage; under 4 °C refrigeration, pH exceeds 8.0 after 10 days. Under identical storage durations, shrimp wrapped with rBC-T_{10} maintain lower pH values, proving the synergistic fresh-preserving effect of low temperature and RPE. Visual observation of shrimp appearance further supports this conclusion: after 3 days at 25 °C, BC-T packaged shrimp turn gray with softened abdominal muscle and abundant black spots on shrimp tails, while rBC-T_{10} samples retain intact body shapes with far fewer dark lesions. After 10 days of cold storage at 4 °C, BC-T wrapped shrimp emit mild putrid odor with sticky body surfaces, whereas rBC-T_{10} samples remain odorless without obvious spoilage. The visual changes perfectly match pH testing data, demonstrating superior fresh-keeping capacity of rBC-T_{10} compared with pure TOCNF films. The dual antioxidant and bacteriostatic activity of RPE polyphenols can suppress spoilage microorganism proliferation and mitigate oxidative degradation of proteins and lipids to delay seafood spoilage processes. In addition, the dense fiber network of rBC-T_{10} reduces oxygen and water vapor transmittance, further inhibiting microbial metabolism and enhancing barrier fresh-preserving performance.

Notably, rBC-T_{10} exhibits visual color response throughout storage under both ambient and cold conditions. Alkaline substances released by spoiled shrimp alter the micro-pH environment of composite films and trigger color changes of embedded RPE polyphenols, realizing real-time visual indication of seafood spoilage. Integrating the barrier advantage of TOCNF matrix and dual bioactivity of rose polyphenols, rBC-T_{10} demonstrates remarkable application potential in aquatic product fresh packaging, especially effective shelf-life extension under refrigerated conditions, providing solid laboratory data for industrial application in chilled meat and aquatic active packaging.

4 Conclusions

Inspired by the structural advantage of natural cellulose skeleton and functional characteristics of plant polyphenols, this research adopted bacterial cellulose as raw material, utilized TEMPO oxidation system to synthesize TOCNF, blended with rose polyphenol extract RPE and fabricated multifunctional rBC composite films via vacuum filtration technology. The composite membranes integrate outstanding mechanical strength, thermal stability, full-spectrum UV shielding capacity and selective antibacterial fresh-preserving activity, and the intrinsic correlation between micro-structure and macroscopic performance was systematically elaborated:

Phenolic hydroxyl groups of RPE form abundant hydrogen bonds with hydroxyl and carboxyl groups on TOCNF surfaces, realizing homogeneous polyphenol dispersion inside nanofiber networks without damaging ordered cellulose skeleton, and endowing composite films with multiple functional properties.

Elevating TEMPO oxidation temperature promotes complete oxidation of cellulose chains, and TOCNF prepared at 60 °C (BC-60) achieves a carboxyl content of 1.2 mmol/g.

rBC composite films drastically reduce UV light transmittance and realize full UV blocking within 200–400 nm wavelength range, with enhanced shielding performance along with increased RPE addition dosage.

rBC composite films display prominent selective antibacterial activity against E. coli yet negligible inhibition on S. aureus. When the mass ratio of BC-60 to RPE reaches 1:10, the resultant rBC-T_{10} film produces an inhibition zone diameter of (13.02±0.29) mm under 0.5 wt% E. coli suspension concentration.

rBC-T_{10} delivers excellent fresh-preserving capacity for aquatic products. After storage under both 25 °C and 4 °C conditions, shrimp samples packaged with rBC-T_{10} maintain lower pH values than those wrapped by pure BC-60 TOCNF films. Moreover, rBC-T_{10} undergoes distinct color transformation with shrimp spoilage, achieving visual real-time indication of seafood freshness.

References

[1] Hou C Y. Preparation and Performance Study of High Performance Nanocellulose Materials[D]. Wuxi: Jiangnan University, 2023.
[2] Zhou Z, Zhao H W, Han Z L, et al. High Strength and Toughness Transparent Bacterial Cellulose Film[J]. Journal of Cellulose Science and Technology, 2024, 32(1): 1-8.
[3] Song B, Shi Y, Lu H L, et al. Preparation and Characteristics of a Paper-based Bacterial Cellulose Microfiltration Membrane[J]. Transactions of China Pulp and Paper, 2015, 30(4): 32-37.
[4] Chen T, Zhang M, Deng B Y, et al. Research Progress of Nanocellulose Research in the Field of Food[J]. Transactions of China Pulp and Paper, 2024, 40(2): 48-57.
[5] Tian S H, Luo Q, He P, et al. Preparation of Intelligent Colorimetric Paper Strip Based on SKN@TOCN/CGG and Its Application in Freshness Detection of Chicken Breast[J]. Transactions of China Pulp and Paper, 2024, 39(4): 124-133.
[6] Okita Y, Saito T, Isogai A. Entire Surface Oxidation of Various Cellulose Microfibrils by TEMPO-mediated Oxidation[J]. Biomacromolecules, 2010, 11(6): 1696-1700.
[7] Fukuzumi H, Saito T, Iwata T, et al. Transparent and High Gas Barrier Films of Cellulose Nanofibers Prepared by TEMPO-mediated Oxidation[J]. Biomacromolecules, 2009, 10(1): 162-165.
[8] Miao X, Hua W, Li Y, et al. Extraction of Cellulose Nanofibrils from Pine Sawdust by Integrated Chemical

Pretreatment[J]. Heliyon, 2024, 10(3): e25355.
[9] Qin H, Deng X Q, Li B C, et al. Volatiles, Polysaccharides and Total Polyphenols in Chinese Rose Tea Infusions and Their Antioxidant Activities[J]. Journal of Food Processing and Preservation, 2018, 42(1): e13323.
[10] Zhu R, Wang L, Chao A, et al. Effect and Mechanisms of Thermal Sterilization Methods on the in Vitro Phenolic Bioaccessibility of Rose Tea with Milk[J]. Food Chemistry, 2024, 458: 140248.
[11] Bekar E. Valorization of Quince by-products Using Natural Deep Eutectic Solvents (NADES): Extraction and in Vitro Digestion of Phenolic Compounds[J]. Foods, 2023, 14(20): 3507.
[12] Wu H, Lei Y, Zhu R, et al. Preparation and Characterization of Bioactive Edible Packaging Films Based on Pomelo Peel Flours Incorporating Tea Polyphenol[J]. Food Hydrocolloids, 2019, 90: 41-49.
[13] Qin Y, Liu Y, Zhang X, et al. Development of Active and Intelligent Packaging by Incorporating Betalains from Red Pitaya (Hylocereus Polyrhizus) Peel into Starch/Polyvinyl Alcohol Films[J]. Food Hydrocolloids, 2020, 100: 105410.
[14] Otoni C G, Moura D M R, Aouada F A, et al. Antimicrobial and Physical-mechanical Properties of Pectin/Papaya Puree/Cinnamaldehyde Nanoemulsion Edible Composite Films[J]. Food Hydrocolloids, 2014, 41: 188-194.
[15] Isogai A, Zhou Y. Diverse Nanocelluloses Prepared from TEMPO-oxidized Wood Cellulose Fibers: Nanonetworks, Nanofibers, and Nanocrystals[J]. Current Opinion in Solid State and Materials Science, 2019, 23(2): 101-106.
[16] Saito T, Kimura S, Nishiyama Y, et al. Cellulose Nanofibers Prepared by TEMPO-mediated Oxidation of Native Cellulose[J]. Biomacromolecules, 2007, 8(8): 2485-2491.
[17] Sun H, Shao X, Jiang R, et al. Mechanical and Barrier Properties of Corn Distarch Phosphatezein Bilayer Films by Thermocompression[J]. International Journal of Biological Macromolecules, 2018, 118: 2076-2081.
[18] Dong H, Snyder J F, Williams K S, et al. Cation-induced Hydrogels of Cellulose Nanofibrils with Tunable Moduli[J]. Biomacromolecules, 2013, 14(9): 3338-3345.
[19] Isogai A, Saito T, Fukuzumi H. TEMPO-oxidized Cellulose Nanofibers[J]. Nanoscale, 2011, 3(1): 71-85.
[20] Girard L P L, Desjardins P, Unger W E S, et al. Chemical Characterisation of Nitrogen-rich Plasma-polymer Films Deposited in Dielectric Barrier Discharges at Atmospheric Pressure[J]. Plasma Processes and Polymers, 2008, 5(7): 631-644.
[21] Kumar K M, Mahendhiran M, Diaz M C, et al. Green Synthesis of Ce^{3+} Rich CeO_2 Nanoparticles and Its Antimicrobial Studies[J]. Materials Letters, 2018, 214: 15-19.
[22] Silveira E A, Luz S M, Leão R M, et al. Numerical Modeling and Experimental Assessment of Sustainable Woody Biomass Torrefaction via Coupled TG-FTIR[J]. Biomass and Bioenergy, 2021, 146: 105981.
[23] Ono Y, Horikawa Y, Takeuchi M, et al. Distribution of Carboxy Groups in TEMPO-oxidized Cellulose Nanofibrils Prepared from Never-dried Japanese Cedar Holocellulose, Japanese Cedar-callus, and Bacterial Cellulose[J]. Cellulose, 2024, 31(7): 4231-4245.
[24] Huang X, Du L, Li Z, et al. A Visual Bi-layer Indicator Based on Mulberry Anthocyanins with High Stability for Monitoring Chinese Mitten Crab Freshness[J]. Food Chemistry, 2023, 411: 135497.
[25] Han X, Zhang M, Zhang R, et al. Physicochemical Interactions between Rice Starch and Different Polyphenols and Structural Characterization of Their Complexes[J]. LWT, 2020, 125: 109227.
[26] Wu J Z, Yang Y, Li S, et al. Glucose-sensitive Nanoparticles Based on Poly(3-acrylamidophenylboronic acid-block-n-vinylcaprolactam) for Insulin Delivery[J]. International Journal of Nanomedicine, 2019, 14: 8059-8072.
[27] Qin Y. Stability and Application of Active and Intelligent Packaging Films Based on Anthocyanins from Lycium Ruthenicum Murr[D]. Yangzhou: Yangzhou University, 2021.
[28] Shabbir M, Rather L J, Mohammad F. Exploring the Potential of Tannin Based Colorants towards Functional Value Addition of Wool Textiles[J]. Fibers and Polymers, 2019, 20(9): 1812-1819.
[29] Dadvar S, Tavanai H, Dadvar H, et al. UV-protection and Photocatalytic Properties of Electrospun Polyacrylonitrile Nanofibrous Mats Coated with TiO_2 Nanofilm via Sol-Gel[J]. Journal of Sol-Gel Science and Technology, 2011, 59(2): 269-275.
[30] Scorţanu E, Priscariu C, Caraculacu A A. Study of the Mechanical Properties of Dibenzyl-based Polyurethane Containing a Molecularly Dispersed UV Absorber[J]. High Performance Polymers, 2004, 16(1): 113-121.
[31] Feng Y, Li D, Wang Y, et al. Synthesis and Characterization of a UV Absorbent-intercalated Zn-Al Layered Double Hydroxide[J]. Polymer Degradation and Stability, 2006, 91(4): 789-794.
[32] Liu P, Gao C, Han C, et al. Nanosilica-immobilized UV Absorber: Synthesis and Photostability of Polyolefins[J]. Polymer International, 2015, 64(8): 1053-1059.

[33] Ferreyra M L F, Serra P, Casati P. Recent Advances on the Roles of Flavonoids as Plant Protective Molecules after UV and High Light Exposure[J]. Physiologia Plantarum, 2021, 173: 736-749.
[34] Gochev V, Jirovetz L, Wlcek K, et al. Chemical Composition and Antimicrobial Activity of Historical Rose Oil from Bulgaria[J]. Journal of Essential Oil Bearing Plants, 2009, 12(1): 1-6.
[35] Son J Y, Kim T O. Antioxidative and Physiological Activities of Traditional Korean Teas[J]. Korean Journal of Food and Cookery Science, 2011, 27(5): 567-575.
[36] Wang X, Wang C, Zhao J, et al. A Trilaminar Edible Film of Nanocellulose, Konjac Glucomannan, and Curcumin with pH-responsive and Amphiphilic Properties: Preparation, Characterization, and Application[J]. Food Chemistry, 2024, 488: 144913.
[37] Lawal K G, Nazir A, Sundarakani B, et al. Bioactive Biopolymer Films Reinforced with Cellulose Nanocrystals and Green-extracted Polyphenols from Date Seeds for Veal Meat Preservation[J]. International Journal of Biological Macromolecules, 2023, 310: 143275.
[38] Fan S, Wang W, Yang Q, et al. Reinforcement of Chitosan/ Polyvinyl Alcohol Film by Quercetin Self-assembled Nanocrystals for Fresh Meat Preservation[J]. Food Chemistry, 2023, 493: 145826.
[39] Xu Y, Liu Y H, Xu L H. Multifunctional Composite Film of Curcumin Pickering Emulsion Stabilized by Lignocellulose Nanofibrils Isolated from Bamboo Shoot Shells for Monitoring Shrimp Freshness[J]. Carbohydrate Polymers, 2024, 346: 122663.